

# A double wake model for interacting boundary layer methods

## Rajesh Vaithiyanathasamy\*

Energy Research Center of The Netherlands (ECN), Westerduinweg 3, 1755 LE Petten, The Netherlands University of Twente, Drienerlolaan 5, 7522 NB Enschede, The Netherlands

# Hüseyin Özdemir<sup>†</sup> and Gabriele Bedon<sup>‡</sup>

Energy Research Center of The Netherlands (ECN), Westerduinweg 3, 1755 LE Petten, The Netherlands

#### Arne van Garrel§

University of Twente, Drienerlolaan 5, 7522 NB Enschede, The Netherlands

In this study a double wake model is presented for an interacting boundary layer method. The model is described initially by employing only to the inviscid flow equations and compared to the aerodynamic design tools that are including the viscous modelling (XFOIL/RFOIL) as well as to the CFD method  $(SU^2)$  and experimental data on selected airfoils. The details of the implementation of the model into the viscous flow equations are presented. When combined with the integral boundary layer method for the viscous effects, the presented double wake model improves the prediction of pressure distribution as well as the lift coefficients. This is due to the realistic pressure distribution prediction in the separated flows by double wake model. The deficit of interacting boundary layer methods in case of massively separated flows and deep stall regimes can be overcome by use of the proposed double wake model. The improvements in the prediction of the aerodynamic properties of selected airfoils of various thicknesses are shown for both sharp and blunt trailing edges at different operating conditions.

	Nomenclature	$U_{\gamma}$ $U_{inv}$	Induced velocity from vorticity distribution Inviscid velocity
$A_{ci,j}$ $A_{li,j}$	Coefficient matrix of constant strength singularity vortex elements  Coefficient matrix of linear strength singularity vortex elements	$m$ $ar{n}$ $n_i$ Subscr	Mass deficit Transition amplication variable Unit normal to the $i^{th}$ panel
$C_D \\ C_{\tau} \\ C_f \\ C_p \\ C_{\tau EQ}$	Dissipation coefficient Shear stress coefficient Skin friction coefficient Pressure coefficient Equilibrium shear stress coefficient	$egin{array}{c} 0 \ \gamma \ e \ i \ j \end{array}$	value at free stream vorticity distribution value at edge of boundary layer Counter for collocation point counter for panel edge in anticlockwise direc-
$H$ $H^*$ $H_k$ $\Delta H$ $Re_{\theta 0}$	Shape factor Kinetic energy shape parameter Kinetic shape parameter Pressure jump across the secondary wake Critical Reynolds number	SEP $TE$ $Symbo$	tion value at the separation point value at the trailing edge
$Re_{\theta}$ $U$	Momentum thickness Reynolds number Total velocity	$\gamma \ \mu_e$	Vortex strength singularity element Doublet strength singularity element

<sup>\*</sup>M.Sc. Student, Sustainable Energy Technology, rajeshvaithi92@gmail.com

<sup>†</sup>Researcher, Wind Energy Unit, h.ozdemir@cn.nl

<sup>‡</sup>Researcher, Wind Energy Unit, bedon@ecn.nl

<sup>§</sup>Researcher, Engineering Fluid Dynamics Group, a.vangarrel@utwente.nl

 $\sigma$ 

- abla Derivative  $\xi$  Shear layer coordinate  $\phi$  Velocity potential
  - Source strength singularity element Superscripts  $\nu$  iteration counter

#### I. Introduction

Industry standard aerodynamic design tools i.e. (XFOIL¹ or RFOIL²-5) couples a panel method to solve the inviscid flow around the airfoil with an integral boundary layer formulation for viscous flows. The panel method adopts doublet/vortex singularity elements.<sup>6</sup> In the traditional panel methods, a single wake is released from trailing edge. The integral boundary layer equations are then solved using source terms on the airfoil surface and the wake to estimate the boundary layer parameters.<sup>7</sup> The viscous effects are incorporated with the inviscid solution using a viscous-inviscid coupling procedure.

The single wake concept leads to inefficiencies in predictions for separated and stalled flows. The prediction at angles of attack for which separation occurs can be improved by releasing a secondary wake from the separation point. The idea of double wake implementation can be extended to both conventional sharp trailing edge and blunt trailing edge airfoils. Several authors in literature provided different approaches for the double wake modelling. Vezza et al.<sup>8</sup> modelled an unsteady, incompressible separated flow where N+1 linear vortices are considered on N airfoil panels; for the near wake, a panel at separation point and one at the trailing edge are included; for the far wake, discrete vortices model the asymptotically steady separated flow. For moving airfoils, Riziotis and Voutsinas<sup>9,10</sup> modelled unsteady double wake with N sources and two distributed vortices representing attached and separated regions with strong interaction of unsteady boundary layer. The model predicts accurately the separation location up to moderate stall. Zanon<sup>11</sup> adopted Riziotis model for vertical axis wind turbines with modifications in the orientation of near wake panel. Ramos Garcia<sup>12</sup> modelled unsteady 2D flow with linear vortices and a source. This yields to a good agreement for the predicted aerodynamic lift compared to experimental data, while drag is under predicted. Steady double wake for separated flows are modelled by Maskew et al. 13 and Marion et al. 14 with the length of the wake sheets determined by a wake factor and a wake height. Maskew determines the initial wake shape with a parabolic curve whereas Marion considers an experimental wake factor. These models show good agreement with experimental data with some discrepancies in deep stall region.

In this study we present an implementation where the second wake is released from the separation point with initial wake shape defined from induced velocities of linear vortices on airfoil. The inviscid model uses separation point from the experiment. The same model is then integrated into an interacting boundary layer method (i.e. RFOIL) using the source terms for viscous coupling. The separation point required for modelling the second wake is known from a first iteration of viscous simulation.

In the next section (II), the flow equations for inviscid flow region is presented followed by the inviscid double wake model description. Then the viscous flow equations, viscous-inviscid coupling scheme and then the details of the double wake model implementation in interacting boundary layer method are explained. The results are shown in section (III) and the conclusions are given in section (IV).

# II. Double wake model formulation and implementation in interactive boundary layer method

#### II.A. Inviscid formulation

The inviscid flow over airfoils is a potential flow and can be described by using Laplace equation. The continuous mathematical equation is given by,

$$\nabla^2 \phi = 0, \tag{1}$$

where  $\phi$  represents the velocity potential. The total solution to the potential flow can be described as sum of the solutions of the individual elementary flows, using principle of superposition. The elementary flow can be modelled by vortex/doublet singularity elements. The relation between vortex and doublet singularity

element is given by the following relation:

$$\gamma(x) = -\frac{d\mu(x)}{dx},\tag{2}$$

where  $\gamma$  is the vortex singularity element and  $\mu$  represents the doublet singularity element. The surface of the airfoil is modelled using linear vortex singularity element for mimicking inviscid flow as the usage of vortex element is a reasonable choice. Linear elements are used since there is no singularity at the panel edges as with lower order elements. Any higher order elements can be used to increase the accuracy, however requiring a more complex implementation. The induced velocity from vortex singularity element in an inviscid, incompressible, irrotational flow can be describes as,

$$\vec{U}_{\gamma} = \nabla \phi. \tag{3}$$

The airfoil is impermeable to the flow. This property is utilized to obtain the unknown singularity distribution over the airfoil by Neumann boundary condition as given by,

$$\vec{U}_{\gamma}.n_i = 0, \tag{4}$$

where  $n_i$  is the unit normal to the  $i^{th}$  panel representing airfoil surface. The surface geometry of airfoil is divided into N flat panels. The collocation point is chosen to be the midpoint of each panel. For each panel, a linear strength vortex is considered as singularity element with its strength defined at the panel edges. The normal component of the induced velocity at each of the collocation point due to influence of all the linear strength vortices on the airfoil surface is calculated based on Biot-Savart law.<sup>6</sup> Kutta condition is enforced at the trailing edge, such that the flow of the fluid leaving the trailing edge is smooth, to get an unique physical solution and the wake with zero vorticity. The N+1 singularity vortex distribution elements at the panel edges are calculated by means of N+1 boundary conditions. Neumann boundary conditions are imposed on N collocation points at panel midpoints and Kutta condition is expressed as N+1<sup>th</sup> boundary condition. At each collocation point, the linear vorticity influence of every panel on the airfoil surface is taken into account. The imposed Neumann no penetration boundary condition can be written as follows

$$\sum_{j=1}^{N+1} A_{li,j} \gamma_j + (\vec{U}_0.n_i) = 0, \quad \text{for } i = 1 \text{ to } N,$$
(5)

where  $A_{li,j}$  is the coefficient matrix of linear strength singularity vortex elements and  $U_0$  is the freestream velocity. The flow inside the airfoil is stagnant and so the tangential velocity is given by the airfoil surface vorticity, in the absence of source terms.<sup>7</sup> The inviscid pressure coefficient  $(C_p)$  distribution can be calculated from the known vorticity distribution on the airfoil surface and is given by

$$C_p = 1 - \frac{\gamma_j^2}{U_0^2}. (6)$$

The obtained single wake solution for inviscid case depends on the number of panels and their density. To get an accurate solution, natural cubic spline interpolation is employed on the airfoil surface for increasing the number of panels and stretching the grid using distance between the input points as a variable. It is a local method, utilizing many pieces of polynomial for interpolation and hence the high curvature region of airfoil is captured accurately. The panelling on airfoil surface is fixed at 300 panels after comparison with inviscid solution obtained by XFOIL at various angles of attack for different airfoils. One such result is shown in Figure (1). The result of the inviscid formulation is on top of XFOIL, providing reliable estimates therefore enabling to model the secondary wake from the separation point.

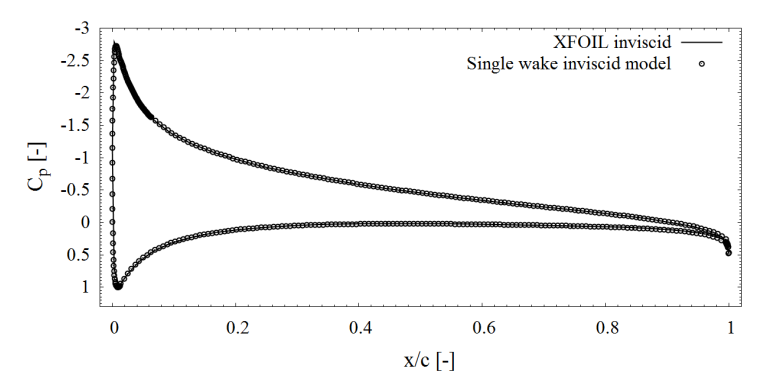


Figure 1: A comparison of  $C_p$  distribution obtained by inviscid formulation and XFOIL inviscid result at angle of attack of  $6^{\circ}$  for NACA0012 airfoil.

#### II.B. Double wake model

Double wake concept models the pressure distribution in the separated region as a result of convected vorticity due to flow separation. Once the separation sets in, formed vorticity (curl of the velocity) in the viscous layer is convected continuously downstream from the beginning of the separation region in the suction side and from the trailing edge pressure side of the airfoil. This convected vorticity can be modelled with a wake sheet emanating from the separation point and another from the trailing edge with vorticity strength. Further, the vorticity is negligible in the separated flow region (i.e. region between two wakes) leading to negligible losses and constant total pressure. Therefore, the flow is assumed to be purely inviscid in this region. This constant pressure region is modelled using the Kutta condition which also makes the flow physical and unique. The modified Kutta condition from that of non-separated flow is considered between the separation point and the trailing edge:

$$\gamma_{N+1} + \gamma_{SEP} = 0, (7)$$

where  $\gamma_{N+1}$  is the vorticity at the pressure side of trailing edge and  $\gamma_{SEP}$  is the vorticity at the separation point. The local vorticity at the trailing edge in the suction side is made zero to accommodate the Kutta condition and to convect the wake towards the side of separation. Moreover, the local vorticity downstream the separation point is made negligible to convect the wake from the separation point downstream, as shown in Figure (2).

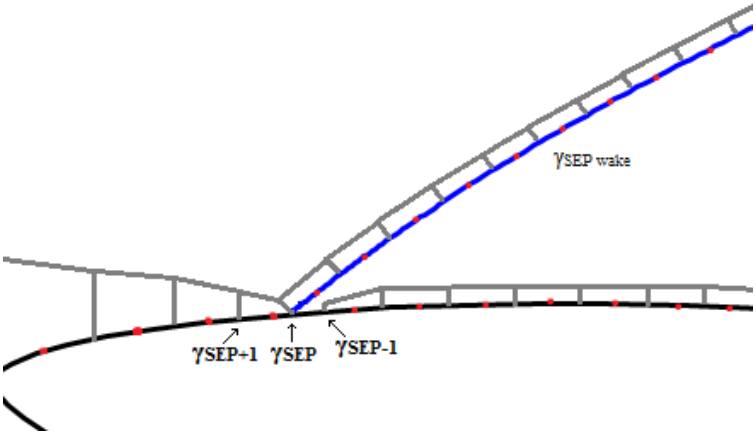


Figure 2: A sketch of the vorticity distribution at the separation point along with the separation point wake (blue line) used as initial condition.

To calculate the influence of the wake on airfoil surface vorticity, the wake shape needs to be determined. The initial shape of the wake in the steady state is determined from the induced velocity of the linear vortices on the airfoil surface along with the contribution of the freestream velocity. Both the wakes at the trailing edge and the separation point are built with panels of increasing size using cosine distribution. This is

because smaller number of increasing size panels is sufficient compared to constant size panels to obtain the similar result. Once the initial shape is estimated, the solution is obtained by applying vorticity of constant strength on the wake panels. The strength of the vortices on the wake is given by,

$$\gamma_{SEP_{wake}} = \gamma_{SEP},\tag{8}$$

$$\gamma_{TE_{wake}} = \gamma_{N+1},\tag{9}$$

where  $\gamma_{SEP_{wake}}$  and  $\gamma_{TE_{wake}}$  represent the vorticity distribution along the secondary and trailing edge wake respectively. The vorticity strengths on the airfoil and wake panels can be iteratively calculated by considering the Neuman boundary condition on the collocation points:

$$\sum_{j=1}^{N+1} A_{li,j} \gamma_j + \sum_{j=N+2}^{N+Nw+1} A_{ci,j} \gamma_j + \sum_{j=N+Nw+2}^{N+2Nw+1} A_{ci,j} \gamma_j + (\vec{U}_0.n_i) = 0, \quad \text{for } i = 1 \text{ to } N,$$
(10)

where  $A_{ci,j}$  is the coefficient matrix of constant strength singularity vortex elements. In the first iteration, the total velocity at any point is calculated as the sum of the freestream velocity and the induced velocity from the vorticity on airfoil surfaces as

$$\vec{U} = \vec{U}_0 + \vec{U}_{\gamma_{airfoil}}.\tag{11}$$

For the next iterations, the total velocity is estimated considering the contribution of freestream velocity and those induced from vorticity located on the airfoil surface and on both the wakes:

$$\vec{U} = \vec{U}_0 + \vec{U}_{\gamma_{airfoil}} + \vec{U}_{\gamma_{SEP_{wake}}} + \vec{U}_{\gamma_{TE_{wake}}}, \tag{12}$$

where  $\vec{U}$  represents the total velocity. For subsequent iterations after the initial one, the separation point is forced to be away from the panel edges and the collocation points. The separation point is moved to avoid having one less equation in the system and also singularities of solution scheme. The solution is also not affected as the separation point is moved only to a very small distance and the panel size is also very small. A representation of the initial vorticity distribution is shown in Figure (3).

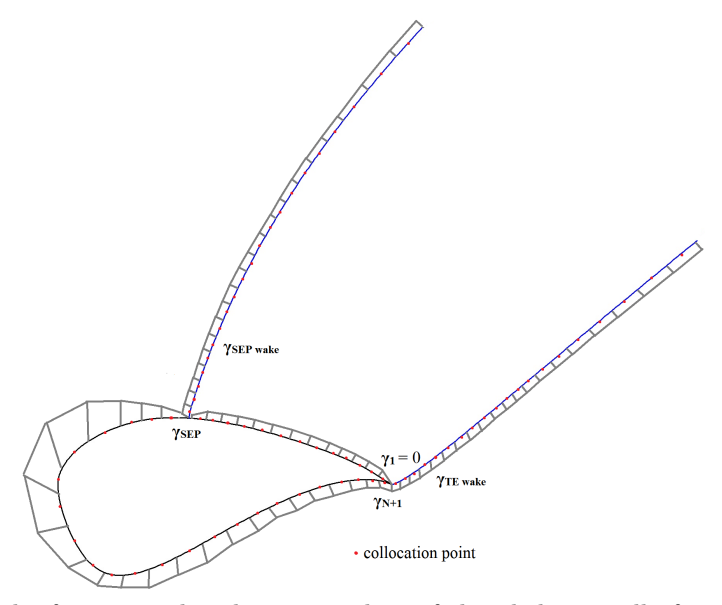


Figure 3: A sketch of vorticity distribution on the airfoil and the initially formed double wake.

The initial near wake panel of the second wake from separation point is at very high angle with respect to the airfoil. This means the flow does not leave the airfoil surface smoothly. The wake shape is recalculated for subsequent iterations based on velocities from airfoil and wake vorticity as given by equation (12) and the solution is iterated with the trailing edge wake and separation wake vorticity influence over airfoil vorticity distribution until the near wake panels from the separation point leaves the airfoil surface smoothly. Further, the accuracy of the solution obtained depends on the chosen number of wake panels and in turn the wake length. The wake panel influence is examined by comparing the calculated  $C_l$  values with 10 to 500 panels on the wake. The number of wake panels for the analysis is fixed to be 300, higher than the number for which no influence on the final solution is registered. The obtained initial wakes geometry and the final wakes after convergence, from separation point and trailing edge is shown in Figure (4) for NACA63415 airfoil operating at an angle of attack of  $16^{\circ}$ . The same is shown in Figure (5) representing near wake region of the initial and the final wakes.

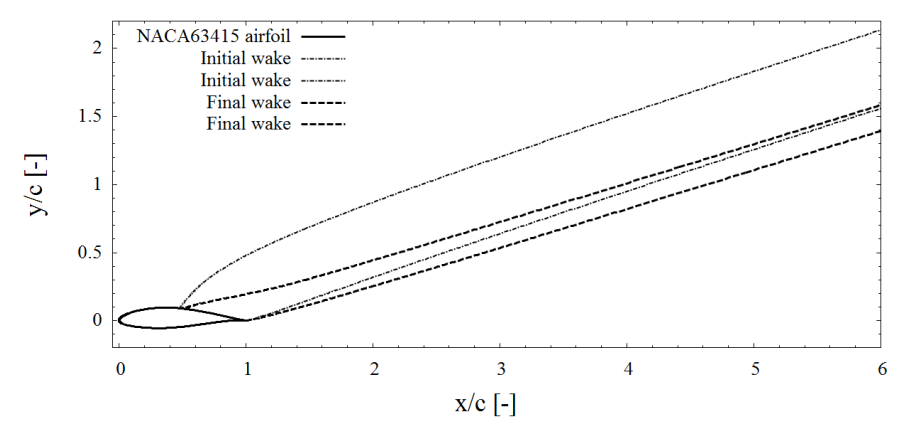


Figure 4: Initial and final wake shape of NACA63415 airfoil for  $\alpha = 16^0$  obtained by inviscid double wake model.

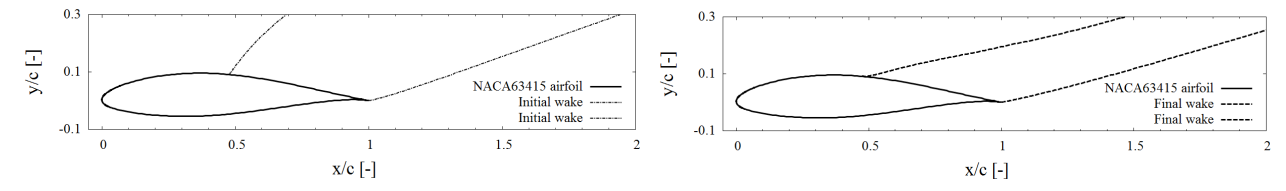


Figure 5: A zoom-in to the initial (left) and final wake shapes of NACA63415 airfoil.

A constant pressure distribution in the separation region on airfoil surface is registered. This value is estimated by considering the modified pressure distribution as described by Maskew et al.:<sup>13</sup>

$$C_p = 1 - \frac{\gamma_j^2}{U_0^2} + \frac{\Delta H}{0.5 \,\rho \, U_0^2},\tag{13}$$

where  $\Delta H$  represents the total pressure jump across the secondary wake and  $\rho$  is the air density. Using Bernoulli's theorem, the total pressure jump in the separation region can be described as follows

$$\Delta H = P_{SEP^{-}} + \frac{\rho}{2} U_{SEP^{-}}^{2} - P_{SEP^{+}} - \frac{\rho}{2} U_{SEP^{+}}^{2}, \tag{14}$$

where  $P_{SEP^+}$ ,  $P_{SEP^-}$  are the local pressures before and after the separation point respectively. Similarly,  $U_{SEP^+}$ ,  $U_{SEP^-}$  are the local velocity before and after the separation point respectively. The wake is a streamline so that there is no static pressure drop across the convected shear layer from the separation point. The total pressure jump across the secondary wake at separation point can be given by

$$\Delta H = \frac{\rho}{2} U_{SEP^{-}}^{2} - \frac{\rho}{2} U_{SEP^{+}}^{2}. \tag{15}$$

The local vorticity at the separation point is the difference in local velocities before and after the separation. According to Riziotis<sup>10</sup> the local velocity after separation is zero which leads to

$$\gamma_{SEP} = U_{SEP^+}. (16)$$

Hence, the total pressure jump in the separation region is given as follows

$$\Delta H = -\rho \frac{\gamma_{SEP}^2}{2}.\tag{17}$$

The result of the double wake model is shown in the section (III) and the implementation of the validated model in viscous flow model is shown in subsequent sections.

#### II.C. Viscous formulation

To simulate the viscous effects in the boundary layer, the two equations model is used with von Karman momentum equation and kinetic energy shape parameter equation in the integral form to avoid Goldstein singularity and to determine the displacement thickness  $\delta^*$  and momentum thickness  $\theta$ :

$$\frac{d\theta}{dx} + (H+2)\frac{\theta}{U_e}\frac{dU_e}{dx} = \frac{C_f}{2},\tag{18}$$

$$\theta \frac{dH^*}{dx} + (1 - H)H^* \frac{\theta}{U_e} \frac{dU_e}{dx} = 2C_D - H^* \frac{C_f}{2}, \tag{19}$$

where H is the shape factor,  $U_e$  is the velocity at the edge of the boundary layer,  $C_f$  is the skin friction coefficient,  $C_D$  is the dissipation coefficient and  $H^*$  is the kinetic energy shape parameter. Furthermore,  $e^n$  transition and lag-entrainment equations<sup>15</sup> are used for laminar/ transition and turbulent flows respectively:

$$\frac{d\bar{n}}{d\xi}(H_k, \theta) = \frac{d\bar{n}}{dRe_{\theta}}(H_k) \frac{f_1(H_k) + 1}{2} f_2(H_k) \frac{1}{\theta},$$

$$\bar{n}(\xi) = \int_{\xi_0}^{\xi} \frac{d\bar{n}}{d\xi} d\xi,$$
(20)

where,  $\xi_0$  is at  $Re_{\theta} = Re_{\theta 0}$ .  $\xi$  is the shear layer coordinate,  $Re_{\theta}$  is the momentum thickness Reynolds number,  $Re_{\theta 0}$  is the critical Reynolds number,  $\bar{n}$  is the transition amplification variable,  $H_k$  is the kinetic shape parameter,  $f_1$  and  $f_2$  are the empirical functions of  $H_k$ . Finally the rate equation for the shear stress  $C_{\tau}$  is given by the following equation

$$\frac{\delta}{C_{\tau}} \frac{dC_{\tau}}{d\xi} = 4.2(C_{\tau EQ}^{1/2} - C_{\tau}^{1/2}),\tag{21}$$

where  $C_{\tau}$  and  $C_{\tau EQ}$  are the shear stress coefficient and equilibrium shear stress coefficient respectively. The  $e^n$  transition model is used to predict transition location and to determine associated losses with bubble size. The lag-entrainment equation is used for turbulent flow to incorporate the response of shear stress to the flow. To close the system of equations, six empirical closure sets are used (for details see<sup>2,3</sup>).

#### II.D. Viscous-Inviscid coupling

The viscous model is coupled with inviscid solution incorporating the mass deficits, which are modelled considering source singularity elements. The source singularity elements are distributed on the airfoil surface and the wake. The mass deficit is a function of inviscid layer edge velocity and displacement thickness from viscous calculation. The relation between the source singularity elements and the mass deficit is given by

$$\sigma = \frac{dm}{dx} = \frac{d(U_{edg}\delta^*)}{dx},\tag{22}$$

where  $\sigma$  is the source strength singularity element, m is the mass deficit and  $U_{edg}$  is the velocity at the edge of the boundary layer. The fully simultaneous viscous-inviscid coupling is employed and the unknowns from

both inviscid and viscous formulation are calculated iteratively by Newton-Raphson method with quadratic convergence. The Newton-Raphson solution procedure can be set-up for the system F(X) = 0 as,

$$\delta X^{\nu} = -\frac{\partial F}{\partial X}^{\nu^{-1}} F(X^{\nu}),$$

$$X^{\nu+1} = X^{\nu} + \delta X^{\nu},$$
(23)

where X is a vector of unknowns comprising  $C_{\tau}/\bar{n}$ ,  $\theta$ , m and a rotational term. F(X) represents the system of equations (18), (19), (20), (21) and rotational effects equation.  $\nu$  is the iteration counter. From the mass term, the  $\delta^*$  and  $U_{edg}$  can be calculated.

#### II.D.1. Implementation of double wake model in interacting boundary layer models

The interactive boundary layer methods like XFOIL/RFOIL combining the panel method and integral boundary layer (IBL) equations becomes inefficient when separation occurs. The integral boundary layer equations along with the empirical closure sets cannot handle the complex vortex shedding with the separated flow, as the closure sets are based on equilibrium flow assumption and become invalid. To solve the above mentioned discrepancy, the proposed double wake method is implemented in one of interacting boundary layer methods, and here it is chosen to be RFOIL.

The airfoil coordinates are the required input in RFOIL which are discretised into panels based on density and distribution parameters. The potential flow solution is calculated from panel method and is used to model the inviscid wake and initialize the Integral Boundary Layer (IBL) equations. In RFOIL (also in XFOIL), there are three viscous sweeps (i.e. marching through all grid points) namely initialization sweep, direct or inverse mode sweep based on value of H to avoid Goldstein singularity and sweep to solve the fully simultaneous coupling using Newton system (details in section II.D) to calculate the boundary layer properties and the aerodynamic coefficients. The viscous sweeps are iterated until the required convergence level is achieved. For non-separated flows, wake geometry is calculated again using the converged viscous solutions and the IBL equations are initialized. The solution procedure is repeated until convergence to obtain the final result.

In order to implement the double wake model in interacting boundary layer method, separation point is required and is calculated from the first sweep of the viscous boundary layer calculation. Based on the value of H and depending on the type of flow i.e. laminar, transition or turbulent, the separation point is determined. With this separation point input, the above mentioned double wake model in section(II.B) is used to model the pressure distribution in the separated flow region. The total pressure jump between the non-separated region and the separated flow region is accounted in the velocity distribution calculated from double wake method based on the work of Maskew et al.<sup>13</sup> and is given as:

$$\gamma_{new} = 1 - \sqrt{\gamma_j^2 + \gamma_{SEP}^2}. (24)$$

The flow inside the airfoil is stagnant and so the tangential velocity can be given by the airfoil surface vorticity, in the absence of source terms as described by Drela. The calculated  $\gamma_{new}$  in the separated flow region from the double wake model is combined with the velocity distribution in non-separated flow region from potential flow solution based on panel method. A new velocity distribution over the airfoil surface is obtained as an initial condition to carry out boundary layer sweep. As a result, a new wake shape is defined and the IBL equations are re-initialized. The inviscid wake geometry used in double wake method and the viscous wake used for second iteration in single wake method are shown in the Figure (6).

It can be seen that the initial inviscid wake geometry used in double wake approach to initialize the IBL equations and distribute source terms to couple inviscid and viscous solutions are different than that of the viscous wake in single wake method. The updated wake approach as a result of establishing the constant pressure region from double wake method aids in improved lift prediction and lift to drag polar as shown in the viscous results section (III.B).

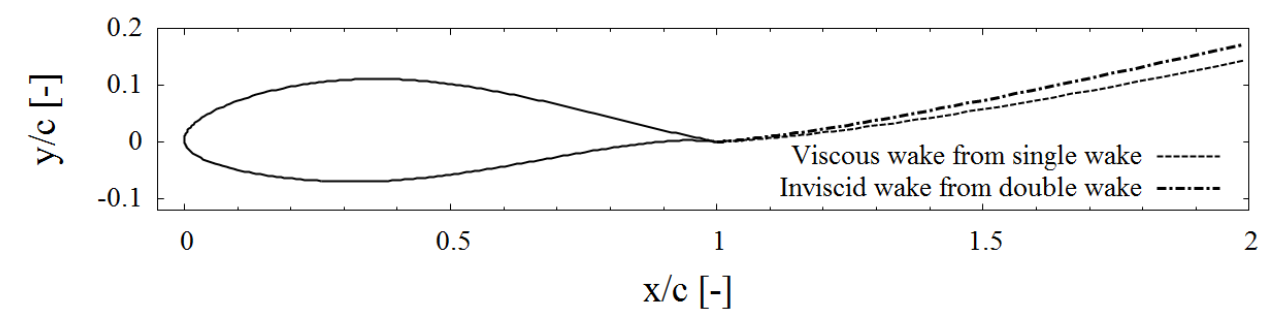


Figure 6: Wake geometry of NACA 63<sub>3</sub>418 airfoil at  $Re = 3 \cdot 10^6$  and at  $\alpha = 16^0$ 

## III. Results

Two types of results are shown, namely, inviscid results: using the inviscid double wake method developed to evaluate the robustness of the double wake approach and conducting preliminary analysis, viscous results: by implementing the double wake approach in one of the interacting boundary layer methods, RFOIL. For the preliminary analysis, the separation point is taken externally from the experimental data for the corresponding angle of attack. For the viscous results, the separation point is taken from the first iteration solution of the tool under consideration (XFOIL/RFOIL).

#### III.A. Inviscid Results

Two conventional trailing edge airfoils namely S826, NACA63415 and a blunt trailing edge airfoil FFA-W3-301 are considered in the analysis. The pressure distribution obtained by the inviscid double wake method is compared to the experimental data<sup>16–18</sup> and also to the viscous numerical results obtained by XFOIL and the open source CFD tool  $SU^2$  (see reference<sup>19</sup>). In this study the numerical solution by  $SU^2$  is obtained by employing BC transition model and Spalart-Allmaras turbulence model for incompressible flows. The converged result after mesh convergence study from CFD is used for comparison. The viscous numerical results by XFOIL and  $SU^2$  are calculated for incompressible flow conditions ( $M_{\infty} = 0$ ).

#### III.A.1. S826 airfoil

Figure (7) shows the comparison of pressure coefficients between the inviscid double wake method with the numerical models CFD, XFOIL and experimental data<sup>16,20</sup> for S826 airfoil at  $Re = 1.0 \cdot 10^5$  and angle of attack of 14.5°. The separation point for the inviscid double wake method is located at x/c = 0.43 and is obtained from experimental data. It can be seen that the inviscid double wake method can replicate result closer to CFD, XFOIL viscous solutions and experimental data in the separation region. However, the peak suction pressure is highly over-predicted as it is an inviscid solution. Further, the release of wake from separation point gives a small oscillation at the separation point.

#### III.A.2. NACA63415 airfoil

Figure (8) shows the comparison of pressure coefficient for NACA63415 airfoil obtained by the inviscid double wake method along with numerical models CFD and XFOIL viscous solutions and experimental data<sup>17</sup> at  $Re = 1.6 \cdot 10^5$  and angle of attack of 16°. The separation point for the inviscid double wake method is located at x/c = 0.475 and is obtained from experimental data. It can be seen that also for this airfoil the inviscid double wake method can replicate result closer to CFD and XFOIL viscous solutions along with experimental data in the separation region. Also, the complete pressure distribution from the inviscid double wake method is also better predicted and closer to experimental data in comparison with the other methods used. It has to be considered that feeding the separation point from experiment gives advantage to the inviscid double wake model. Further, the release of wake from separation point gives a small oscillation at the separation point as in the previous case.

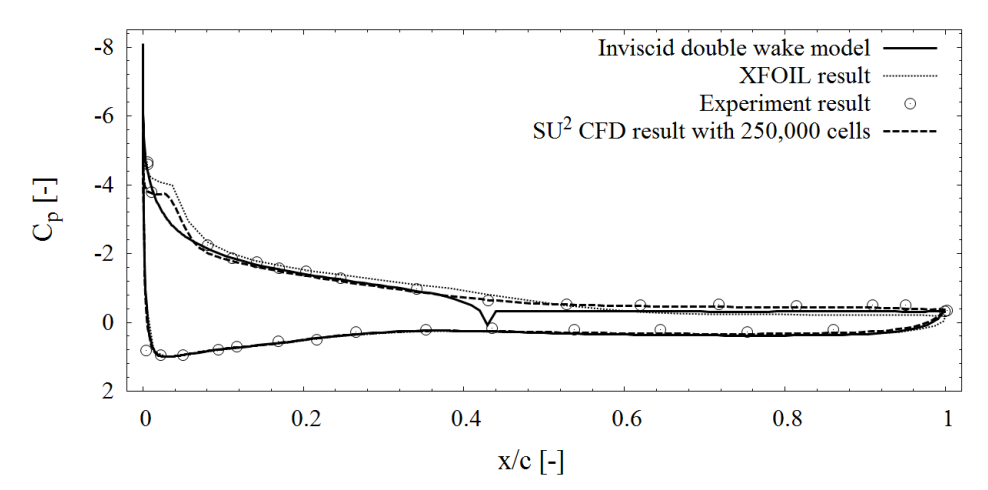


Figure 7: Comparison of pressure coefficient of inviscid double wake method for S826 airfoil with experimental data, CFD and XFOIL viscous solutions at  $Re=1.0 \cdot 10^5$  and at angle of attack of 14.5°.

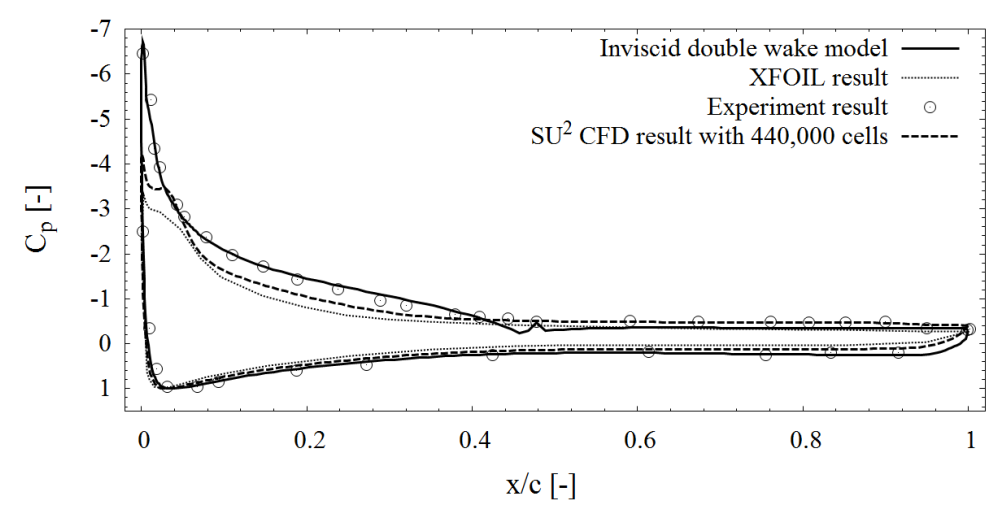


Figure 8: Comparison of pressure coefficient of inviscid double wake method for NACA63415 airfoil with experimental data, CFD and XFOIL viscous solution at Re= $1.6 \cdot 10^5$  and at angle of attack of  $16^{\circ}$ .

#### III.A.3. FFA-W3-301 airfoil

Result for blunt trailing edge airfoil is shown in the Figure (9) using FFA-W3-301 30% thick airfoil. The plot shows the pressure distribution obtained from inviscid double wake model along with the experiment  $^{21}$  and XFOIL results at  $Re=1.6\cdot 10^6$  and angle of attack of  $16.7^\circ$ . The separation point for the inviscid double wake method is located at x/c=0.41 and is obtained from experimental data. It can be seen that the pressure distribution in the separation region can be captured to a very good accuracy when compared to experimental data. The inviscid double wake model gives more accurate result than XFOIL viscous simulation. However, it has to be considered again that feeding the separation point from experiment gives advantage to the inviscid double wake model. The complete pressure distribution also matches with that of the experimental data and better predicted than XFOIL viscous solution, although it is an inviscid method. Further, the release of wake from separation point gives a small oscillation at the separation point.

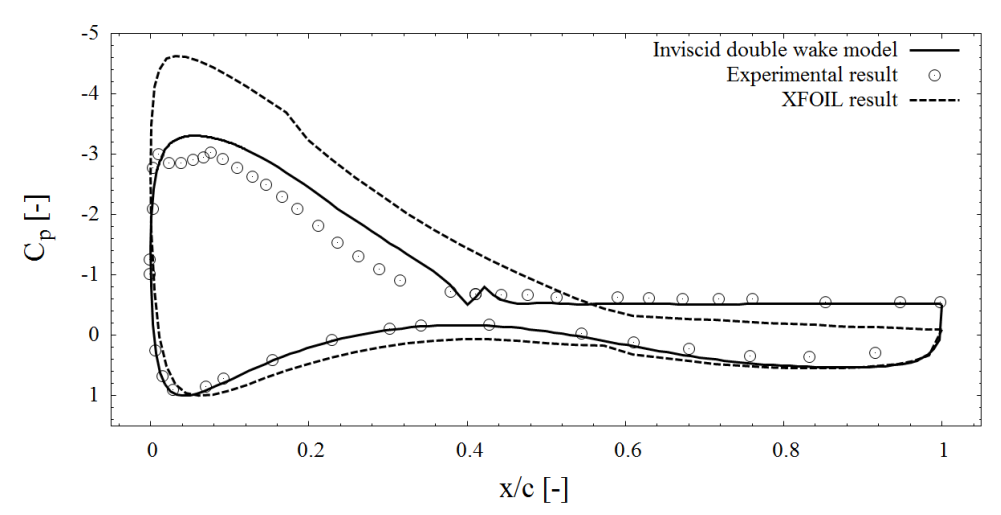


Figure 9: Comparison of pressure coefficients for FFA-W3-301 airfoil of inviscid double wake model with experiment and XFOIL result at  $Re = 1.6 \cdot 10^6$  and angle of attack of 16.7°.

In all the cases presented in this section, there is a small hump at the separation point where the Kutta condition is forced. This is due to the presence of gradient of the velocity distribution before it becomes constant in the separated flow region. Considering the gradient to account for the total pressure jump can mitigate this deficiency. Since, the main aim is to develop the double wake model for interacting boundary layer methods, with the obtained convincing enough results the focus is shifted towards its implementation in interactive boundary layer methods.

#### III.B. Viscous Results

The double wake model implementation in interactive boundary layer method is validated by testing wind turbine airfoils used in various sections of the wind turbine blades namely, in-board, mid- and out-board sections. The tests are done for incompressible flows at  $M_{\infty} = 0$ . Several different airfoils used for wind turbine applications of varying trailing edge thicknesses are studied and few of the cases are presented here to avoid redundancy. The improvement in the prediction of lift coefficients are prominent using double wake implementation. The results of interactive boundary layer method (here RFOIL) with double wake model is compared with the single wake version of RFOIL and latest version of XFOIL(6.99) along with the experimental data ( $^{22-25}$ ) for all the selected airfoils. The details of the airfoils are given in the Table 1.

Airfoils	Max thickness (%)	Trailing edge	$h_{TE}/c$ (%)
AH 93-W-257	25.7	Blunt	0.773
AH 93-W-300	30	Blunt	1.409
AH 94-W-301	30.1	Blunt	1.584
DU 00-W-212	21	Blunt	0.3333
NACA 63 <sub>3</sub> 418	18	Sharp	0
S 809	21	Sharp	0

Table 1: Details of airfoils tested with viscous double wake method.

#### III.B.1. Blunt trailing edge airfoils

Figures (10 - 14) show the results of the test cases with blunt trailing edge airfoils. A wide range of airfoils of maximum thickness ranging from 18% to 30% is tested. Figure (10a), (10b) and (10c) show the plot of lift coefficients, drag coefficients and lift drag polar respectively for AH 93-W-257 airfoil at  $Re = 1.5 \cdot 10^6$ . It can be seen that the lift coefficient with RFOIL double wake model is predicted better than the RFOIL single wake version in the separated, stalled and deep stall region. Also, the complete polar is predicted more accurately than XFOIL and closer to experimental data. The drag coefficients remains the same as that of

the RFOIL single wake version. This leads to good prediction of lift to drag coefficient (polar plot) with the RFOIL double wake model compared to other numerical methods. Similar results of improved lift prediction can be interpreted for different airfoils AH 93-W-300, AH 94-W-301 and DU 00-W-212 at various operating conditions. The operating conditions are chosen based on the publicly available experimental results. The drag coefficients are not shown in the result for these airfoils as they remain the same as that of the RFOIL with single wake model. Figure(11) shows the plot of lift coefficients and lift drag polar for AH 93-W-300 airfoil at  $Re = 1.5 \cdot 10^6$ . Figures (12, 13) show similar plots for AH 94-W-301 airfoil at two different operating conditions namely  $Re = 1.5 \cdot 10^6$  and  $Re = 2.5 \cdot 10^6$ . In all the cases for both airfoils, the lift coefficient prediction is accurate when compared to experimental data than the previous version of RFOIL with single wake model, in the separated, stalled and in the deep stalled regime. Similarly, Figure (14) describes the result obtained for DU 00-W-212 airfoil at  $Re = 3 \cdot 10^6$ . The trend of the lift coefficient is well captured with the viscous double wake model along with accurate prediction of  $C_{l_{max}}$ . Also, the convergence is extended into deep stall region.

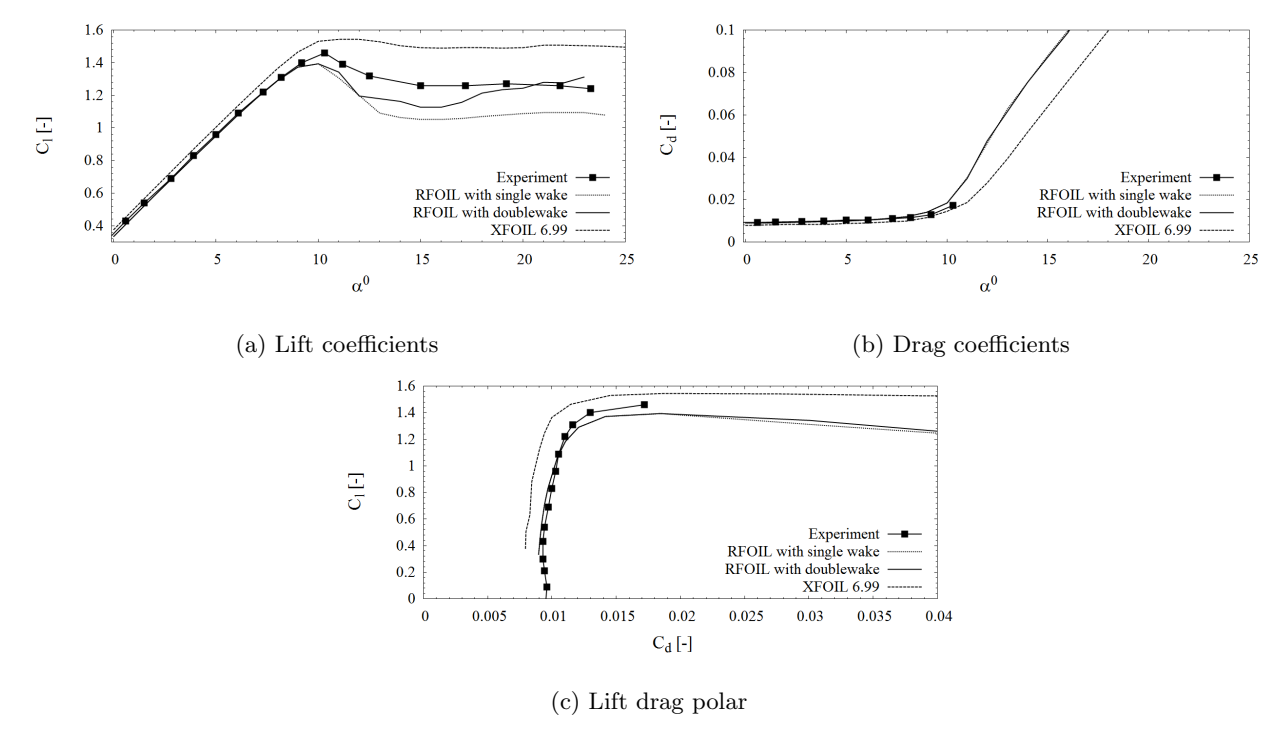


Figure 10: Comparison of lift coefficients, drag coefficients and lift drag polar for AH 93-W-257 airfoil at  $Re = 1.5 \cdot 10^6$ .

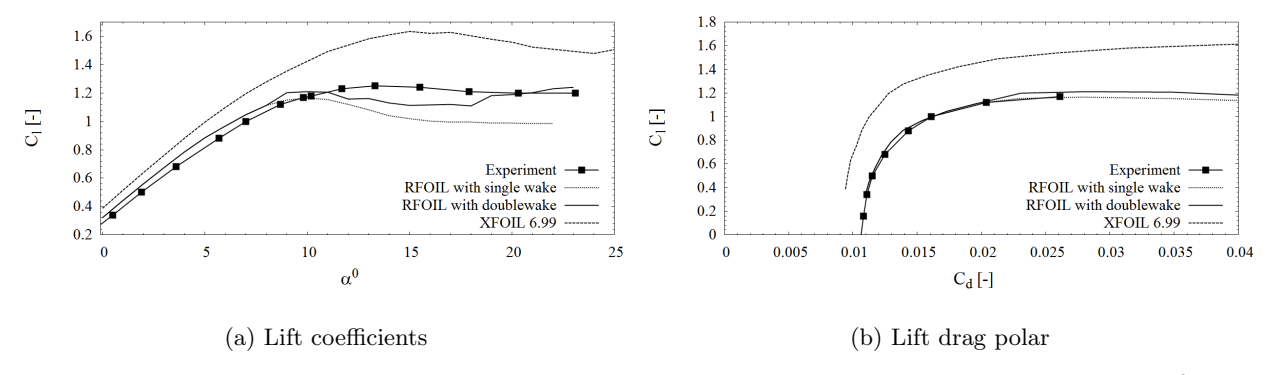


Figure 11: Comparison of lift coefficients and lift drag polar for AH 93-W-300 at  $Re = 1.5 \cdot 10^6$ .

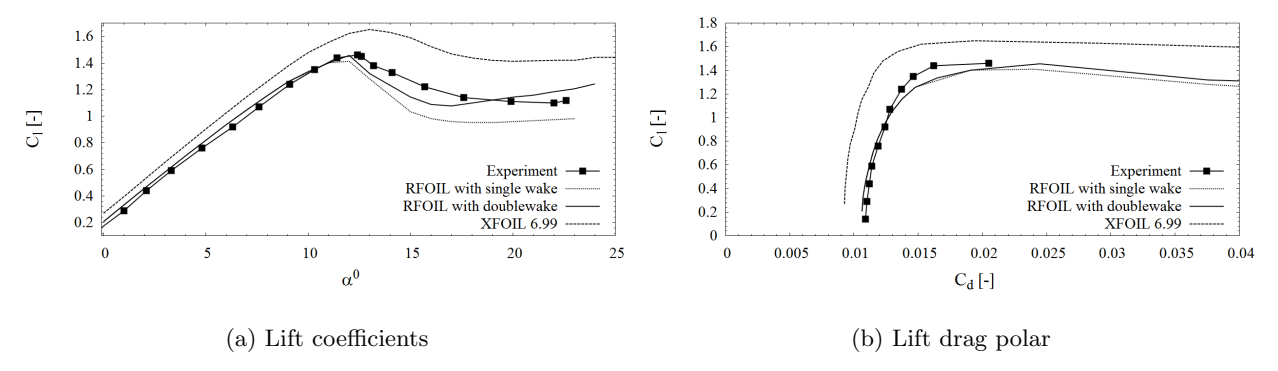


Figure 12: Comparison of lift coefficients and lift drag polar for AH 94-W-301 at  $Re = 1.5 \cdot 10^6$ .

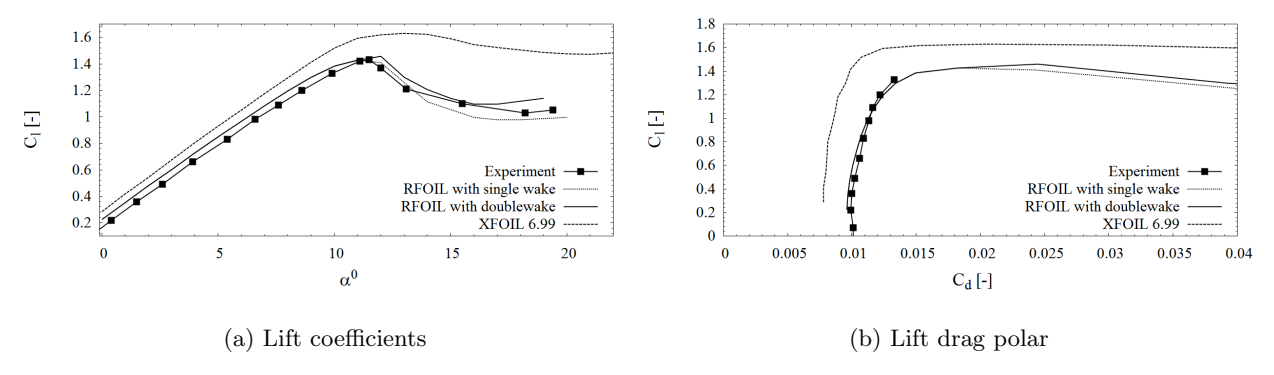


Figure 13: Comparison of lift coefficients and lift drag polar for AH 94-W-301 at  $Re = 2.5 \cdot 10^6$ .

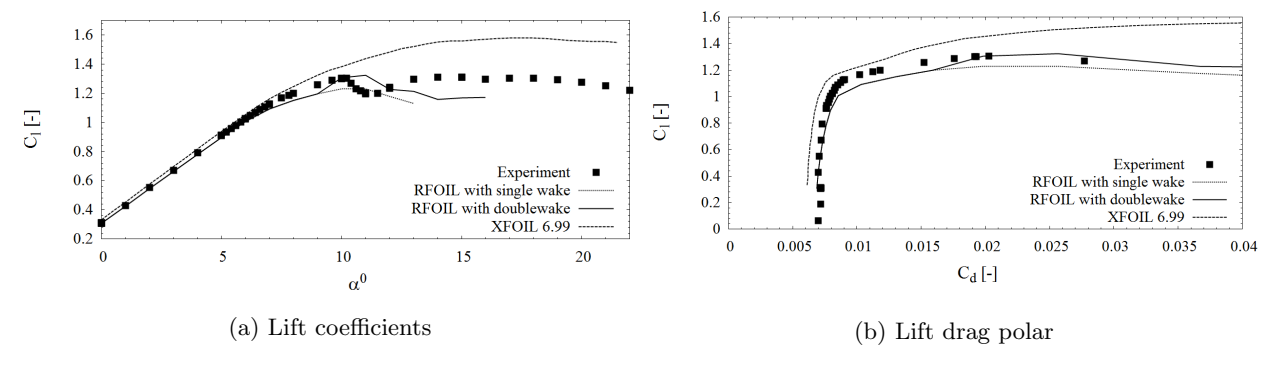


Figure 14: Comparison of lift coefficients and lift drag polar for DU 00-W-212 at  $Re = 3 \cdot 10^6$ .

#### III.B.2. Sharp trailing edge airfoils

This section shows results of two differently profiled sharp trailing edge airfoils namely NACA  $63_3-418$  and S809 of thickness 18% and 21% respectively. Figure(15) shows the plot of lift coefficients and lift drag polar for NACA  $63_3-418$  airfoil at  $Re=3\cdot 10^6$ . It can be seen that the lift prediction for NACA  $63_3-418$  is improved with double wake model and closer to experimental data compared to single wake method of RFOIL and XFOIL. Further, the RFOIL double wake method predicts accurate lift coefficients in the deep stall region where the XFOIL fails to converge and the RFOIL single wake method under predicts the lift coefficient. Similar results of improved lift prediction are obtained for S809 airfoil except in deep stall region where the lift is over predicted. The plot of lift polar and lift to drag polar for S809 airfoil is shown in the Figure(16) for  $Re=1.5\cdot 10^6$ .

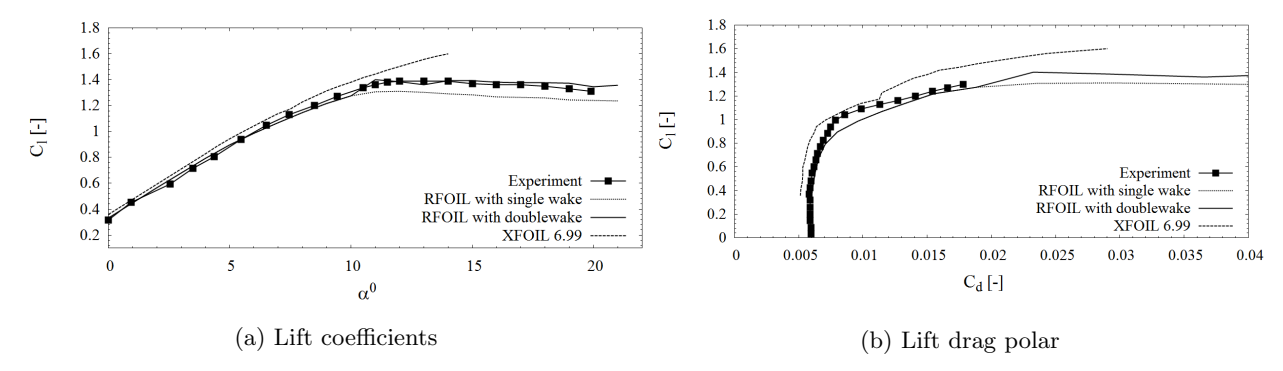


Figure 15: Comparison of lift coefficients and lift drag polar for NACA  $63_3 - 418$  at  $Re = 3 \cdot 10^6$ .

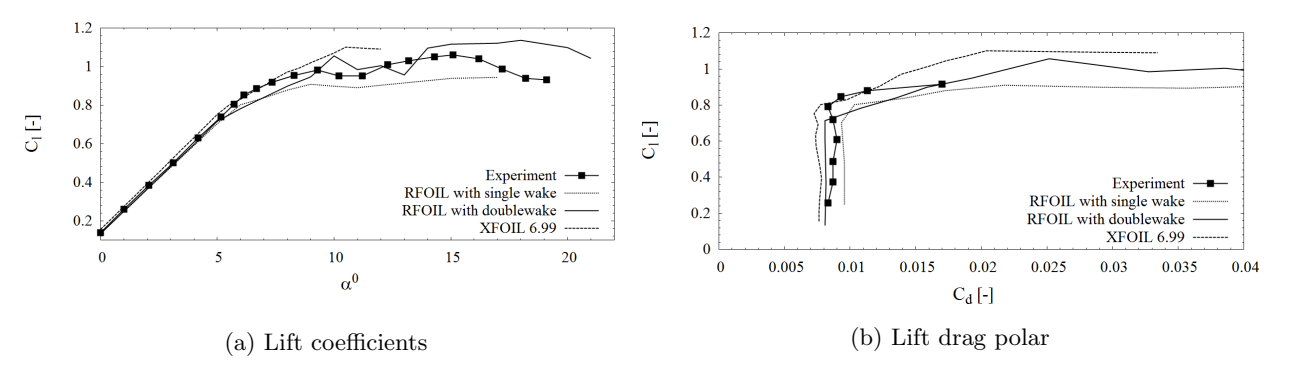


Figure 16: Comparison of lift coefficients and lift drag polar for S809 at  $Re = 1.5 \cdot 10^6$ .

#### IV. Conclusions

The present study focuses on the lift prediction improvement by including a double wake model to an integral boundary layer method. The implementation provides an updated wake definition which allows the creation of a realistic wake shape.

The inviscid results from the preliminary analysis shows that the viscous effects can be predominantly captured by the inviscid double wake method with some discrepancies in predicting peak suction pressure and pressure at separation point. A realistic pressure distribution in the separated region is described.

When combined with the integral boundary layer method for the viscous effects, this model improves the prediction of pressure distribution as well as the lift coefficients for all the airfoils tested. This is due to the realistic pressure distribution prediction in the separated flows by double wake model. The lift prediction is improved by implementing the double wake model in an interacting boundary layer method for the airfoils of various thickness, different profiles and for both sharp and blunt airfoils at different operating conditions. This shows that the deficit of interacting boundary layer methods in case of massively separated flows and deep stall regimes can be overcome by use of double wake model. In this study RFOIL is chosen to implement the suggested double wake method but in general this method is applicable to all XFOIL/RFOIL like interacting boundary layer methods.

#### Acknowledgements

This work has been performed within the Design for Reliable Power Performance (D4REL) project granted by the Dutch Top Consortium for Knowledge and Innovation in Offshore Wind (TKI Wind op Zee) under number TKIW02007 and the AVATAR project, which is initiated by the European Energy Research Alliance (EERA) and carried out under the FP7 program of the European Union.

#### References

<sup>1</sup>Drela, M., "XFOIL: An Analysis and Design System for Low Reynolds Number Airfoils," Low Reynolds Number Aero-dynamics, Springer Berlin Heidelberg, 1989, pp. 1–12.

<sup>2</sup>van Rooij, R., "Modification of the boundary layer calculation in RFOIL for improved airfoil stall prediction," Tech. rep., Delft University of Technology, Report IW-96087R, Delft, The Netherlands, 1996.

<sup>3</sup>Bosschers, J., "Modelling of Rotational Effects with a 2-D Viscous-Inviscid Interaction Code," Tech. rep., NLR Contract Report, CR 96521 C, 1997.

<sup>4</sup>Ramanujam, G., Özdemir, H., and Hoeijmakers, H., "Improving Airfoil drag Prediction," *Journal of Aircraft*, Vol. 53, 2016, pp. 1844–1852.

<sup>5</sup>Ramanujam, G. and Özdemir, H., "Improving Airfoil Lift Prediction," 35th Wind Energy Symposium, No. AIAA 2017-1999 in AIAA SciTech Forum, Grapevine, Texas, 9-13 January 2017.

<sup>6</sup>Katz, J. and Plotkin, A., Low-speed aerodynamics, Cambridge University Press, 2001.

<sup>7</sup>Drela, M., Two-dimensional transonic aerodynamic design and analysis using the Euler equations, Ph.D. thesis, Massachusetts Institute of Technology, 1985.

<sup>8</sup>Vezza, M. and Galbraith, R. A. M., "An inviscid model of unsteady aerofoil flow with fixed upper surface separation," *International Journal for Numerical Methods in Fluids*, Vol. 5, No. 6, 1985, pp. 577–592.

<sup>9</sup>Voutsinas, S. G. and Riziotis, V. A., "A viscousinviscid interaction model for dynamic stall simulations on airfoils," 37th Aerospace Sciences Meeting and Exhibit, 1999, pp. 154–163.

<sup>10</sup>Riziotis, V. A. and Voutsinas, S. G., "Dynamic stall modelling on airfoils based on strong viscous - inviscid interaction coupling," *International Journal for Numerical Methods in Fluids*, Vol. 56, 2008, pp. 185–208.

<sup>11</sup>Zanon, A., A vortex panel method for vawt in dynamic stall, Ph.D. thesis, Università degli Studi di Udine, 2011.

<sup>12</sup>Ramos García, N., Unsteady Viscous-Inviscid Interaction Technique for Wind Turbine Airfoils, Ph.D. thesis, Technical University of Denmark, 2011.

<sup>13</sup>Maskew, B., Vaidyanathan, T. S., Nathman, J., and Dvorak, F. A., "Prediction of Aerodynamic Characteristics of Fighter Wings at High Angles of Attack," Tech. rep., Office of Naval Research, N00014-82-C-0354, Arlington, VA, USA, 1984.

<sup>14</sup>Marion, L., Ramos García, N., and Sørensen, J. N., "Inviscid double wake model for stalled airfoils," *Journal of Physics: Conference Series*, Vol. 524, No. 1, 2014.

<sup>15</sup>Drela, M. and Giles, M. B., "Viscous-Inviscid Analysis of Transonic and Low Reynolds Number Airfoils," *American Institute of Aeronautics and Astronautics Journal*, Vol. 25, No. 2, 1986, pp. 1–9.

<sup>16</sup>Aksnes, N. Y., "Performance Characteristics of the NREL S826 Airfoil," M.Sc. Thesis - Norwegian University of Science and Technology, 2015.

<sup>17</sup>Bak, C., Fuglsang, P., Johansen, J., and Ioannis, A., "Wind Tunnel Tests of the NACA 63-415 and a Modified NACA 63-415 Airfoil," Tech. rep., Risø National Laboratory R-1193(EN), Roskilde, Denmark, 2000.

<sup>18</sup>Somers, D. M. and Tangler, J., "Design and Experimental Results for the S825 Airfoil," Tech. Rep. NREL/SR-500-36345, NREL, National Renewable Energy Laboratory, January 2005.

<sup>19</sup>Palacios, F., Colonno, M. R., Aranake, A. C., Campos, A., Copeland, S. R., Economon, T. D., Lonkar, A. K., Lukaczyk, T. W., Taylor, T. W. R., and Alonso, J. J., "Stanford University Unstructured (SU2): An open-source integrated computational environment for multi-physics simulation and design." *AIAA*, January 2013.

<sup>20</sup>Sagmo, K. F., Bartl, J., and Sætran, L., "Numerical simulations of the NREL S826 airfoil," *Journal of Physics: Conference Series*, Vol. 753, 2016.

<sup>21</sup>Fuglsang, P., Antoniou, I., Dahl, K. S., and Madsen, H. A., "Wind tunnel tests of the FFA-W3-241, FFA-W3-301 and NACA 63-430 airfoils," Tech. Rep. Risø-R-1041(EN), Risø National Laboratory, December 1998.

<sup>22</sup>Althaus, D., "Stuttgarter Profilkatalog II Niedriggeschwindigkeitsprofile," 1996.

<sup>23</sup>Abbott, H. and von Doenhoff, A. E., "Measurements NACA in LTT- Langley," Tech. Rep. 422, 1949.

 $^{24} {\it Franck}, B., Sørensen, N., Johansen, J., and Fuglsang, P., "Wind Turbine Airfoil Catalogue," Tech. Rep. Risø-R-1280(EN), Risø National Laboratory, August 2001.$ 

<sup>25</sup>Yilmaz, O. C., Pires, O., Manolesos, M., and Ferreira, C. S., "Blind Test Campaign," Tech. Rep. D2.10, ECN Wind Energy, Petten, May 2015.